

Phase transitions and domain stabilities in biaxially strained (001) SrTiO₃ epitaxial thin films

G. Sheng, Y. L. Li, J. X. Zhang, S. Choudhury, Q. X. Jia et al.

Citation: *J. Appl. Phys.* **108**, 084113 (2010); doi: 10.1063/1.3488636

View online: <http://dx.doi.org/10.1063/1.3488636>

View Table of Contents: <http://jap.aip.org/resource/1/JAPIAU/v108/i8>

Published by the [American Institute of Physics](#).

Related Articles

Ferroelectric and electrical characterization of multiferroic BiFeO₃ at the single nanoparticle level
Appl. Phys. Lett. **99**, 252905 (2011)

Defect enhanced optic and electro-optic properties of lead zirconate titanate thin films
AIP Advances **1**, 042144 (2011)

Ultrafast switching of ferroelastic nanodomains in bilayered ferroelectric thin films
Appl. Phys. Lett. **99**, 182906 (2011)

Piezoresponse force microscopy observation of domain switching in Bi_{3.15}Nd_{0.85}Ti₃O₁₂ thin film prepared by pulsed laser deposition
J. Appl. Phys. **110**, 054105 (2011)

Atomic mechanism of electric dipole formed at high-K: SiO₂ interface
J. Appl. Phys. **109**, 094502 (2011)

Additional information on J. Appl. Phys.

Journal Homepage: <http://jap.aip.org/>

Journal Information: http://jap.aip.org/about/about_the_journal

Top downloads: http://jap.aip.org/features/most_downloaded

Information for Authors: <http://jap.aip.org/authors>

ADVERTISEMENT

**AIPAdvances**

Submit Now

**Explore AIP's new
open-access journal**

- **Article-level metrics
now available**
- **Join the conversation!
Rate & comment on articles**

Phase transitions and domain stabilities in biaxially strained (001) SrTiO₃ epitaxial thin films

G. Sheng,^{1,a)} Y. L. Li,² J. X. Zhang,^{1,b)} S. Choudhury,³ Q. X. Jia,⁴ V. Gopalan,¹
D. G. Schlom,⁵ Z. K. Liu,¹ and L. Q. Chen¹

¹Department of Materials Science and Engineering, The Pennsylvania State University, University Park, Pennsylvania 16802, USA

²Pacific Northwest National Laboratory, Richland, Washington 99352, USA

³Department of Materials Science and Engineering, University of Wisconsin, Madison, Wisconsin 53706, USA

⁴Center for Integrated Nanotechnologies, Los Alamos National Laboratory, Los Alamos, New Mexico 87545, USA

⁵Department of Materials Science and Engineering, Cornell University, Ithaca, New York 14853, USA

(Received 18 April 2010; accepted 10 August 2010; published online 29 October 2010)

We applied phase-field approach to investigate both ferroelectric and antiferrodistortive transitions in (001) SrTiO₃ epitaxial thin films that are strained biaxially. A domain/phase stability diagram of “misfit strain-temperature” was constructed for equibiaxially strained (001) SrTiO₃ thin films, which exhibits significant differences from previous diagrams obtained using thermodynamic analysis of a single domain. For unequibiaxially strained (001) SrTiO₃ thin films, “misfit strain-misfit strain” domain stability diagrams at several representative temperatures were obtained. The predicted phase transitions, domain stabilities, and domain structures in three different SrTiO₃ thin films under either equibiaxial or unequibiaxial strains agree well with experimental observations. © 2010 American Institute of Physics. [doi:10.1063/1.3488636]

I. INTRODUCTION

SrTiO₃ is an incipient ferroelectric in its pure, unstressed form but has a ferroelectric instability manifested by its large dielectric constants at low temperature.¹ It is also well established that bulk SrTiO₃ crystals undergo a cubic to tetragonal antiferrodistortive (AFD) transition at 105 K in a stress free state, which is associated with staggered rotations of the TiO₆ octahedra around one of the cubic axes.^{2–5} The properties of SrTiO₃ are extremely sensitive to dopants and external perturbations. Ferroelectricity can be induced as a result of small concentrations of dopants,⁶ isotopic substitutions in the oxygen octahedra,⁷ or mechanical pressure.^{8,9} The development of thin film technologies has provided additional ways of inducing ferroelectricity in SrTiO₃ films. Significant enhancement of Curie temperatures (T_c) induced by in-plane misfit strain in SrTiO₃ thin films was experimentally achieved^{10–15} and theoretically predicted by thermodynamic calculations^{15–17} and first-principles calculations.¹⁸ The “misfit strain-temperature” domain stability diagrams predicted by thermodynamics^{15–17} exhibit various ferroelectric and AFD phases, depending on both temperature and misfit strain. However, all the published diagrams from thermodynamic analysis^{15–17} are determined by minimizing the Helmholtz free energy density in terms of temperature, polarization, and AFD structural order parameter under a single domain assumption. During a structural or ferroelectric phase transition, it is inevitable that multiple domains or heterophase structures form due to the degeneracy of domain

states and the release of strain energy. Moreover, the variations in the reported values of bulk properties and the Landau energy coefficients from different literature sources led not only to a wide range of possible transition temperatures at a given strain but also to different ferroelectric states thus different stability diagrams.

Recently, a modified Landau–Devonshire thermodynamic potential for SrTiO₃ is developed,¹⁹ which made it possible to fully understand the existing experimental observations of ferroelectric/AFD states in epitaxial SrTiO₃ thin films.^{12–15} In the past decade, phase-field model has been applied to predicting domain stability, structure, and evolution in a number of ferroelectric thin film systems under various mechanical and electrical boundary conditions.^{20–24} For SrTiO₃ thin films, both the ferroelectric and AFD domain morphologies at a number of specific temperature and strain states were also predicted using phase-field method.¹⁷ However, a complete domain stability diagram taking into consideration of multiphase and multidomain is still lacking. Thus in the present work, we first construct a misfit strain-temperature domain stability diagram for the equibiaxially strained (001) SrTiO₃ thin films using phase-field method and compare it with previous diagrams determined from thermodynamics^{15–17} and first-principles.^{18,25} Then we extend the model to study the domain stabilities under unequibiaxial strains, corresponding to the cases of SrTiO₃ thin films grown on orthorhombic substrates like DyScO₃ (Ref. 12) and GdScO₃.¹³ Isothermal misfit strain diagrams, i.e., the “misfit strain-misfit strain” stability diagrams at several representative temperatures are presented. Finally, we demonstrate the predicted phase transitions, domain stabilities, and domain morphologies of three SrTiO₃ thin films grown on

^{a)}Electronic mail: shengguang@psu.edu.

^{b)}Current address: Research and Development, Carpenter Technology Corporation, Reading, PA 19601.

different substrates with either equibiaxial or unequibiaxial strain states that have been studied experimentally. It can be seen that the predicted phase transitions and domain states in all three available SrTiO₃ thin films agree very well with all the experimental observations.

II. SIMULATION DETAILS

In the phase-field model of strained pseudocubic (001) SrTiO₃ thin film, the spontaneous polarization $\mathbf{p} = (p_1, p_2, p_3)$ and the structural order parameter $\mathbf{q} = (q_1, q_2, q_3)$ are chosen as the order parameters to describe a proper ferroelectric transition and an AFD transition, respectively. The structural order parameter \mathbf{q} is related to the linear oxygen displacement that corresponds to the simultaneous out-of-plane rotation of the TiO₆ octahedra around one of the fourfold symmetry axes. The temporal and spatial evolutions of the two order parameters \mathbf{p} and \mathbf{q} are governed by the time dependent Ginzburg-Landau equations:

$$\frac{\partial p_i(\mathbf{x}, t)}{\partial t} = -L_p \frac{\delta F}{\delta p_i(\mathbf{x}, t)}, \quad i = 1, 2, 3, \quad (1)$$

$$\frac{\partial q_i(\mathbf{x}, t)}{\partial t} = -L_q \frac{\delta F}{\delta q_i(\mathbf{x}, t)}, \quad i = 1, 2, 3, \quad (2)$$

where L_p and L_q are the kinetic coefficients related to the domain mobilities of \mathbf{p} and \mathbf{q} , respectively. The total free energy F includes the bulk free energy, elastic deformation energy, domain wall energy, and electrostatic energy, i.e.,

$$F = \int \int_V [f_{\text{bulk}}(p_i, q_i) + f_{\text{elas}}(p_i, q_i, \varepsilon_{ij}) + f_{\text{wall}}(p_{i,j}, q_{i,j}) + f_{\text{elec}}(p_i, E_i)] d^3x, \quad (3)$$

where V is the volume of the film and $d^3x = dx_1 dx_2 dx_3$. A fourth-order polynomial in the components of both order parameters is employed to describe the bulk free energy density $f_{\text{bulk}}(p_i, q_i)$ (Refs. 16 and 17) under the stress-free condition:

$$\begin{aligned} f_{\text{bulk}}(p_i, q_i) = & \alpha_1(p_1^2 + p_2^2 + p_3^2) + \alpha_{11}(p_1^4 + p_2^4 + p_3^4) \\ & + \alpha_{12}(p_1^2 p_2^2 + p_2^2 p_3^2 + p_3^2 p_1^2) + \beta_1(q_1^2 + q_2^2 + q_3^2) \\ & + \beta_{11}(q_1^4 + q_2^4 + q_3^4) + \beta_{12}(q_1^2 q_2^2 + q_2^2 q_3^2 + q_3^2 q_1^2) \\ & - t_{11}(p_1^2 q_1^2 + p_2^2 q_2^2 + p_3^2 q_3^2) \\ & - t_{12}[p_1^2(q_2^2 + q_3^2) + p_2^2(q_1^2 + q_3^2) + p_3^2(q_1^2 + q_2^2)] \\ & - t_{44}(p_1 p_2 q_1 q_2 + p_2 p_3 q_2 q_3 + p_3 p_1 q_3 q_1), \end{aligned} \quad (4)$$

where α_{ij} , β_{ij} are the Landau coefficients and t_{ij} is the coupling coefficient of p and q .

In a biaxially strained SrTiO₃ film, the elastic energy density with the formation of the ferroelectric and/or AFD domain is given by

$$f_{\text{elas}}(p_i, q_i, \varepsilon_{ij}) = \frac{1}{2} c_{ijkl} e_{ij} e_{kl} = \frac{1}{2} c_{ijkl} (\varepsilon_{ij} - \varepsilon_{ij}^0) (\varepsilon_{kl} - \varepsilon_{kl}^0), \quad (5)$$

where c_{ijkl} is the elastic stiffness tensor, e_{ij} is the elastic strain, ε_{ij}^0 is the stress free strain as a result of ferroelectric and AFD transitions:

$$\varepsilon_{ij}^0 = Q_{ijkl} p_k p_l + \Lambda_{ijkl} q_k q_l, \quad (6)$$

where Q_{ijkl} is the electrostrictive coefficient representing the coupling between the strain and polarization, and Λ_{ijkl} is the linear-quadratic coupling coefficient between strain and structural order parameter. $\varepsilon_{ij} = e_{ij} + \varepsilon_{ij}^0$ is the total strain. Here both ε_{ij} and ε_{ij}^0 are defined using the pseudocubic phase as the reference. The details of the calculation of the total strain ε_{ij} in a (001)-oriented film under biaxial in-plane strains are described in Ref. 20.

The domain wall energy is calculated through

$$f_{\text{wall}}(p_{i,j}, q_{i,j}) = \frac{1}{2} (G_p p_{i,j} p_{i,j} + G_q q_{i,j} q_{i,j}), \quad (7)$$

where G_p and G_q are the domain wall energy coefficients and $p_{i,j} = \partial p_i / \partial x_j$, $q_{i,j} = \partial q_i / \partial x_j$.

The electrostatic energy $f_{\text{elec}}(p_i, E_i)$, induced by spatially inhomogeneous spontaneous polarizations, is calculated by²⁶

$$f_{\text{elec}}(p_i, E_i) = -\frac{\varepsilon_0 \kappa_{ij}}{2} E_i E_j - E_i p_i, \quad (8)$$

where E_i is the electric field component. In the absence of an external electric field,

$$f_{\text{elec}}(p_i, E_i) = -\frac{1}{2} E_i p_i \quad (9)$$

which is essentially the depolarization energy within an inhomogeneous domain structures due to the presence of domain walls, assuming that the top and bottom surfaces are charge-compensated and thus the depolarization energy due to the average polarization within the crystal is assumed to be zero. The electric displacement D_i is related to the electric field as

$$D_i = \varepsilon_0 \kappa_{ij} E_j + p_i, \quad (10)$$

where κ_{ij} is the relative dielectric permittivity of the film and was suggested to take the value of its paraelectric background.^{27,28} Here we assume isotropic dielectricity, i.e., $\kappa = \kappa_{11} = \kappa_{22} = \kappa_{33}$ and $\kappa_{ij} = 0 (i \neq j)$.

For the short-circuit boundary condition, we have $\phi_1 = \phi_2 = \phi_0$, if the electric potential ϕ_i is specified as ϕ_1 on the film bottom surface and as ϕ_2 on the top surface, and

$$E_i = -\phi_{,i}. \quad (11)$$

The electrostatic potential can be obtained by solving the following electrostatic equilibrium equation:

$$D_{i,i} = 0, \quad \text{or} \quad (12a)$$

$$\varepsilon_0 \kappa (\phi_{,11} + \phi_{,22} + \phi_{,33}) = p_{1,1} + p_{2,2} + p_{3,3}. \quad (12b)$$

Equation (12) is numerically solved under the described boundary conditions. Consequently, the electrostatic energy (the depolarization energy) can be obtained.

In this work, a (001)-oriented SrTiO₃ thin film on an orthorhombic substrate is considered. A rectangular coordinate system, $\mathbf{x} = (x_1, x_2, x_3)$ is set up with the x_1 , x_2 , and x_3 axes along the [100], [010], and [001] crystallographic directions, respectively. The average film/substrate misfit strains $e_{s1} = \bar{\varepsilon}_{11}$ and $e_{s2} = \bar{\varepsilon}_{22}$ are along the in-plane x_1 and x_2 axes, respectively. Periodic boundary conditions were applied along the x_1 and x_2 axes. A model size of $256\Delta x \times 256\Delta x$

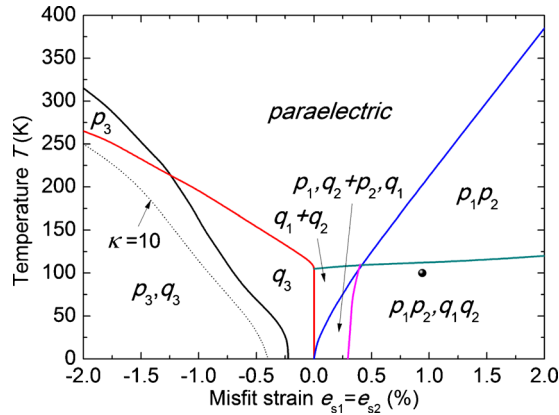


FIG. 1. (Color online) Misfit strain-temperature domain stability diagram of $(100)_p$ -oriented SrTiO_3 thin films. The black dot indicates the experimental strain $e_{s1}=e_{s2}=0.94\%$.

$\times 36\Delta x$ is used with Δx being the grid spacing. The thickness of the film is $20\Delta x$. The kinetic coefficient in Eq. (1) is taken as $L_q/L_p=180$. The gradient energy coefficients $G_q/G_p=0.012$ and $G_p/G_0=0.4$ where G_0 is related to the magnitude of Δx through $\Delta x=\sqrt{G_0/\alpha_0}$ and $\alpha_0=|\alpha_1|$. The short-circuit boundary condition is employed to calculate the dipole-dipole interactions. We performed a series of simulations under different biaxial strains to investigate the domain stabilities under either equibiaxial or unequibiaxial strain states. To study the effect of depolarization field on the Curie temperature, we compare the simulation results using two very different relative dielectric constants: $\kappa=1000$ (simulating the case of nearly compensated domain walls by unspecified free charges)¹⁷ and a background dielectric constant $\kappa=10$.²⁷ The initial polarization and structural order parameter distributions are created by assigning a zero value at each grid plus a small random noise. The material constants used in the simulation are collected from literature^{16,17,19,29} and listed in Ref. 30. Each simulation proceeded for 60 000 time steps or longer (normalized time step is 0.05) until the polarization and/or structure order parameter distributions achieved steadiness.

III. RESULTS AND DISCUSSIONS

Based on the simulations conducted at equibiaxial strain state $e_{s1}=e_{s2}$ ranging from -2% to 2% , we constructed the misfit strain-temperature domain stability diagram for (001) SrTiO_3 thin films, as shown in Fig. 1. Only nonzero components of polarizations and AFD structural order parameters of the stable phases are labeled in the corresponding regions. For example, q_1+q_2 represents tetragonal $(q_1, 0, 0) + (0, q_2, 0)$ AFD domain, p_1p_2 the orthorhombic $(p_1, p_2, 0)$ ferroelectric domain, and p_1, q_2+p_2, q_1 the coexistence of both ferroelectric $(p_1, 0, 0) + (0, p_2, 0)$ and AFD $(q_1, 0, 0) + (0, q_2, 0)$ domains. We examined the effect of the dielectric constant on the predicted Curie temperatures (T_c). It is found there is no significant change in the predicted T_c under tensile strains using different dielectric constants as the polarizations are always developed in-plane thus no depolarization field is generated perpendicular to the film surfaces. While under compressive strains, the T_c predicted from κ

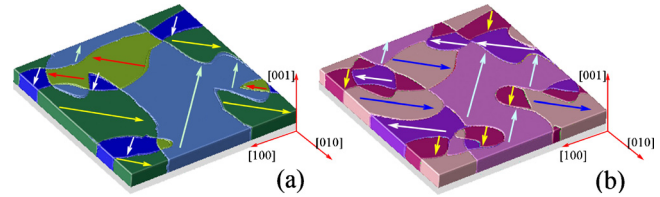


FIG. 2. (Color online) Domain morphologies of SrTiO_3 thin films strained at $e_{s1}=e_{s2}=0.94\%$ at 100 K: (a) ferroelectric domain (b) AFD structure domain.

$=10$ (the dashed line) is about 30–50 K lower than that from a higher dielectric constant $\kappa=1000$, due to the relatively large depolarization field, which will compensate the out of plane polarization to reduce the T_c .

Although the predicted strain dependent transition temperatures assuming $\kappa=1000$ are similar to the results from thermodynamic predictions which entirely ignored the depolarization field,^{16,17} significant differences exist on the predicted domain stabilities. First, the current diagram suggests SrTiO_3 is not ferroelectric under zero strain condition down to the ground state (0 K), which is consistent with both established theories^{1,31} and experiments.^{1,31,32} Second, it is demonstrated that at relatively small tensile strain and low temperature, both polarizations and AFD structural order parameters develop along the pseudocubic $[100]_p/[010]_p$ (subscript p means “pseudocubic”) in-plane axes, i.e., a ferroelastic (q_1+q_2) or ferroelectric $(p_1q_2+p_2q_1)$ twin structure. As the strain magnitude increases, there is a rotation from $[100]_p/[010]_p$ to $[110]_p/[1\bar{1}0]_p$ for both polarization and AFD structure order parameters, indicating a transition from $p_1q_2+p_2q_1$ domain state to p_1p_2, q_1q_2 state, as shown in the diagram. This symmetry dependency on strain is also predicted by both thermodynamics¹⁶ and first-principles calculations.²⁵ In this work, the critical strain separated this two phase regions is around 0.3% at 0 K, which is between the values from thermodynamics¹⁶ (0.1%) and first-principles²⁵ (0.442%). Moreover, the diagram from thermodynamic analysis using an earlier Landau-Devonshire potential¹⁶ demonstrated that a very small compressive strain between -0.022% and -0.05% stabilizes p_1p_2, q_3 phase, i.e., the coupling of ferroelectric p_1p_2 phase and AFD q_3 phase, when temperature is lower than 30 K. Our thermodynamic calculation using the updated potential obtained a similar phase stability in this narrow region, however, phase-field simulations showed that only AFD q_3 phase is stable. (Fig. 1)

In an earlier experimental study, both optical second harmonic generation (SHG) and confocal scanning optical microscopy (CSOM) measurements demonstrated that a 500 Å thick (001) SrTiO_3 thin film on an (101) -oriented DyScO_3 substrate with biaxial strain $e_{s1}=e_{s2}=0.94\%$ (Refs. 12 and 17) exhibits a $[110]_p/[1\bar{1}0]_p$ polar state, which is consistent with our phase diagram. To further compare with experiments, the ferroelectric and AFD structural domain morphologies of SrTiO_3 thin film at $e_{s1}=e_{s2}=0.94\%$ and $T=100$ K are shown in Fig. 2. The four colors used to depict the films in Figs. 2(a) and 2(b) represent the four $[110]_p$ variants. The directions of the corresponding order parameter

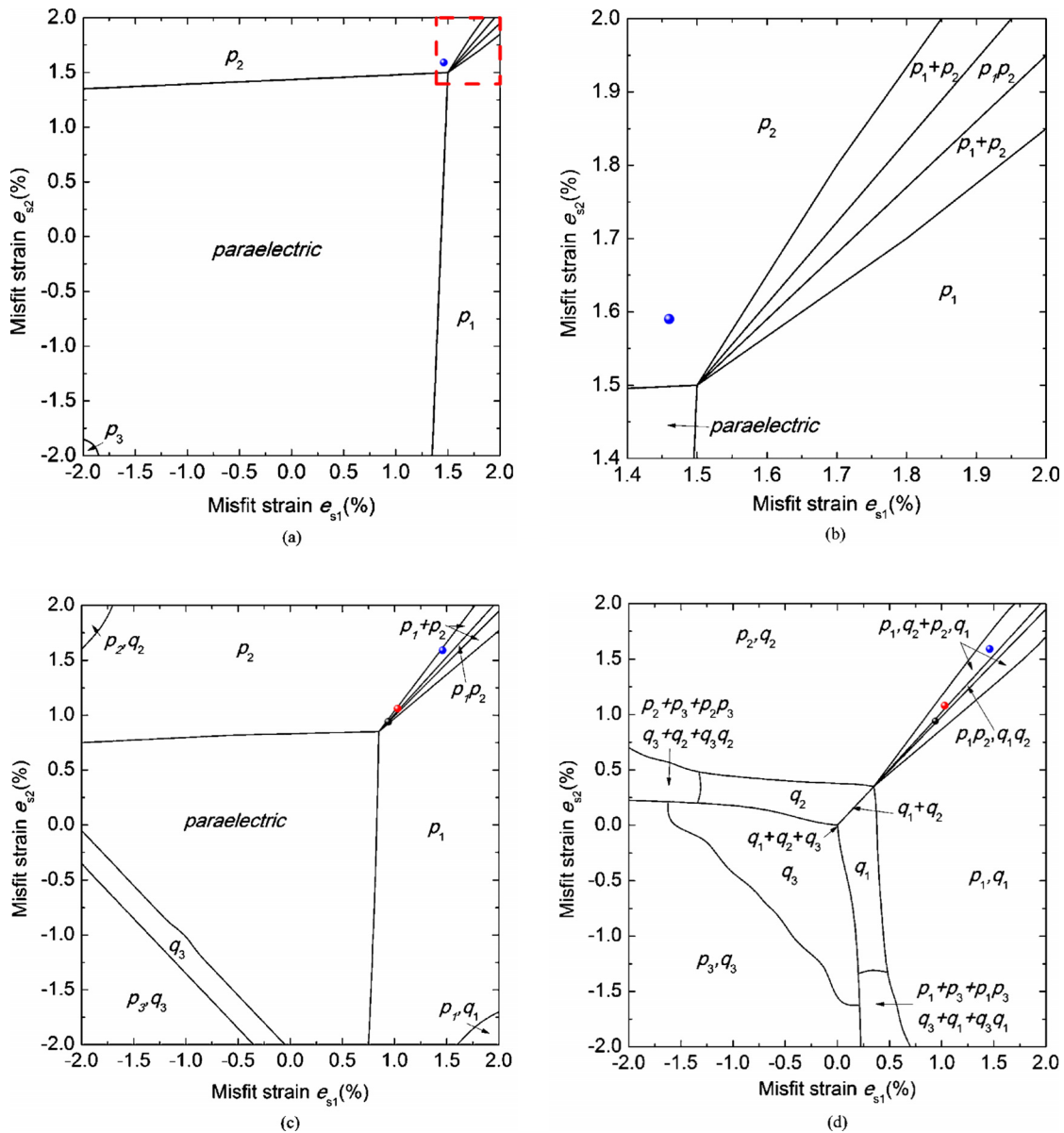


FIG. 3. (Color online) Misfit strain-misfit strain domain stability diagram of (001) SrTiO₃ films at (a) 300 K, (b) enlargement of the square region in (a) and (c) 200 K, (d) 100 K. The strain states for 3 SrTiO₃ thin films are plotted with different symbols: $e_{s1}=e_{s2}=0.94\%$ (black ●), $e_{s1}=1.03\%$, $e_{s2}=1.06\%$ (red ●), $e_{s1}=1.46\%$, $e_{s2}=1.59\%$ (blue ●).

vector \mathbf{p} or \mathbf{q} on the variants are shown by the arrows. From the domain morphologies, it is evident that the polarization \mathbf{p} and AFD order parameter \mathbf{q} are always parallel to each other along $[110]_p$ in-plane directions. This $[110]_p/[1\bar{1}0]_p$ domain state under a large symmetric tensile strain is also consistent with first-principles calculations.¹⁸

When SrTiO₃ thin films are grown on orthorhombic substrates such as DyScO₃ (Ref. 12) and GdScO₃,¹³ an un-

equibiaxial strain state is generated, which may lead to totally different domain stabilities compared with equibiaxially strained films. To investigate the domain stabilities under un-equibiaxial strains, we also constructed the misfit strain-misfit strain domain stability diagrams at 300, 200, and 100 K, as shown in Figs. 3(a)–3(d). These diagrams reveal a number of unique stable ferroelectric and/or AFD domain phases that could not be stabilized under equibiaxial strains

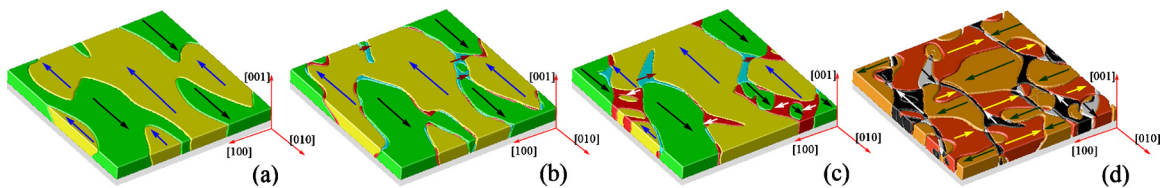


FIG. 4. (Color online) Domain morphologies of SrTiO₃ thin films strained at $e_{s1}=1.46\%$, $e_{s2}=1.59\%$: ferroelectric domains at (a) 300 K, (b) 200 K, (c) 100 K, and (d) AFD structure domain at 100 K.

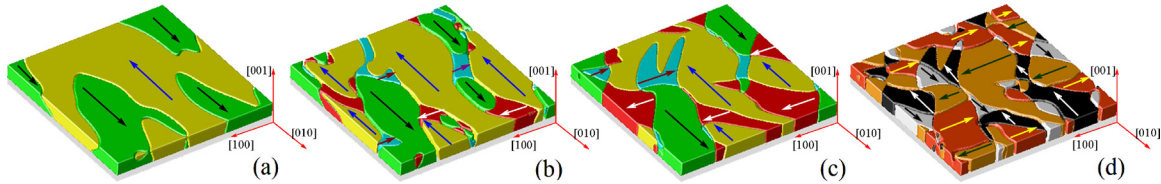


FIG. 5. (Color online) Domain morphologies of SrTiO₃ thin films strained at $e_{s1}=1.03\%$, $e_{s2}=1.06\%$: ferroelectric domains at (a) 212 K, (b) 200 K, (c) 100 K, and (d) AFD structure domain at 100 K.

(Fig. 1). For example, when there is a sufficiently large tensile strain applied along one axis and a smaller tensile strain along the other axis, the stable polarization and/or AFD structural order parameters are along $[100]_p$ and $[010]_p$ in-plane directions, producing a $[100]_p/[010]_p$ twin structure instead of the $[110]_p/[1\bar{1}0]_p$ twins as for the equibiaxial strain case at the same temperature and magnitude of strain. This important difference in the relative stability of the $[110]_p/[1\bar{1}0]_p$ and $[100]_p/[010]_p$ polar states explains why the prior SHG and CSOM measurements of SrTiO₃ films at similar but equibiaxial strains¹⁷ exhibit polar directions along the pseudocubic $[110]_p$ directions while the SHG measurements of asymmetrically strained films shows the $[100]_p/[010]_p$ polar states.^{12,13} Furthermore, if the anisotropy is large enough, the polarization or AFD structure order parameter directions will be along $[100]_p$ or $[010]_p$ direction only, which is again different from the $[100]_p/[010]_p$ or $[110]_p/[1\bar{1}0]_p$ twin structures, as shown in all the three diagrams. Moreover, the stable regions of the $[100]_p/[010]_p$ twin structure, i.e., the p_1+p_2 or $p_1q_2+p_2q_1$ phase area expands with decreasing temperature, indicating a domain twinning from a single variant $[010]_p$ or $[100]_p$ to $[010]_p/[100]_p$ domain structure during a cooling process for the unequibiaxially strained SrTiO₃ thin films. This behavior was also confirmed by SHG measurements in both SrTiO₃ thin films grown on DyScO₃ (Ref. 12) and GdScO₃,¹³ with $e_{s1}=1.03\%$, $e_{s2}=1.06\%$ and $e_{s1}=1.46\%$, $e_{s2}=1.59\%$, respectively. These two experimental strains, as well as the former isotropic case with $e_{s1}=e_{s2}=0.94\%$ are plotted in Figs. 3(a)–3(d) for comparison. On cooling from room temperature, there are three transitions simultaneously for the two unequibiaxially strained SrTiO₃ thin films. The representative domain structures following each of the three transitions are shown in Fig. 4 ($e_{s1}=1.46\%$, $e_{s2}=1.59\%$) and Fig. 5 ($e_{s1}=1.03\%$, $e_{s2}=1.06\%$) and the directions of the corresponding order parameter vectors are indicated by the arrows. The first ferroelectric transition corresponds to the development of a polarization along $[010]$ axis (the higher strain axis) which stabilize the pure p_2 ferroelectric domain [Figs. 4(a) and 5(a)]. The intermediate transition temperature produces the twinning from a single variant $[010]_p$ to $[010]_p/[100]_p$ domain structure [Figs. 4(b) and 5(b)] while the lowest transition temperature corresponds to the AFD transition [Figs. 4(c), 4(d), 5(c), and 5(d)]. It is also noticed that the volume fraction of p_1 domain in Fig. 4(c) is less than that in Fig. 5(c), indicating the larger magnitude of strain anisotropy for SrTiO₃ thin film on GdScO₃ than DyScO₃. The predicted domain stabilities and structures in this work,

as well as the phase transition temperatures reported earlier,^{12,19} agree very well with all existing experimental measurements.^{11–13,17}

IV. SUMMARY

Phase-field simulations were conducted to study the ferroelectric and AFD domain stabilities and structures in strained SrTiO₃ thin films. The obtained misfit strain-temperature domain/phase stability diagram exhibits significant difference from previous diagrams obtained by using thermodynamic analysis. The misfit strain-misfit strain stability diagrams under several representative temperatures were also constructed. These diagrams revealed the important difference between the stabilities of the $[110]_p/[1\bar{1}0]_p$ and $[100]_p/[010]_p$ ferroelectric/AFD phases, and thus explained why the experimental measurements of SrTiO₃ films at equibiaxial strains exhibit $[110]_p$ phase while the equibiaxially strained films shows the $[100]_p/[010]_p$ polar states. The predicted phase transition temperatures and domain structures of the three SrTiO₃ thin films with either equibiaxial or unequibiaxial strains agree well with the available experimental results.

ACKNOWLEDGMENTS

This work was supported by the DOE under the Grant No. DOE DE-FG02-07ER46417 (Sheng and Chen) and NSF under Grant No. IIP-0737759 (Liu). The computer simulations were carried out on the LION clusters at the Pennsylvania State University supported in part by the NSF grants (Grant Nos. DMR-0820404, DMR-0908718, DMR-9983532, and DMR-0122638) and in part by the Materials Simulation Center and the Graduate Education and Research Services at The Pennsylvania State University. The work at Los Alamos National Laboratory was supported by DOE through the LANL/LDRD Program and the Center for Integrated Nanotechnologies (Q. X. Jia).

¹K. A. Müller and H. Burkard, *Phys. Rev. B* **19**, 3593 (1979).

²H. Unoki and T. Sakudo, *J. Phys. Soc. Jpn.* **23**, 546 (1967).

³P. A. Fleury and J. M. Worlock, *Phys. Rev.* **174**, 613 (1968).

⁴G. Shirane and Y. Yamada, *Phys. Rev.* **177**, 858 (1969).

⁵H. Thomas and K. A. Müller, *Phys. Rev. Lett.* **21**, 1256 (1968).

⁶T. Mitsui and W. B. Westphal, *Phys. Rev.* **124**, 1354 (1961).

⁷M. Itoh, R. Wang, Y. Inaguma, T. Yamaguchi, Y.-J. Shan, and T. Nakamura, *Phys. Rev. Lett.* **82**, 3540 (1999).

⁸W. J. Burke and R. J. Pressley, *Solid State Commun.* **9**, 191 (1971).

⁹H. Uwe and T. Sakudo, *Phys. Rev. B* **13**, 271 (1976).

¹⁰M. P. Warusawithana, C. Cen, C. R. Slesman, J. C. Woicik, Y. Li, L. F. Kourkoutis, J. A. Klug, H. Li, P. Ryan, L. P. Wang, M. Bedzyk, D. A. Muller, L. Q. Chen, J. Levy, and D. G. Schlom, *Science* **324**, 367 (2009).

¹¹D. Nuzhnyy, J. Petzelt, S. Kamba, P. Kužel, C. Kadlec, V. Bovtun, M.

- Kempa, J. Schubert, C. M. Brooks, and D. G. Schlom, *Appl. Phys. Lett.* **95**, 232902 (2009).
- ¹²M. D. Biegalski, E. Vlahos, G. Sheng, Y. L. Li, M. Bernhagen, P. Reiche, R. Uecker, S. K. Streiffer, L. Q. Chen, V. Gopalan, D. G. Schlom, and S. Trolier-McKinstry, *Phys. Rev. B* **79**, 224117 (2009).
- ¹³A. Vasudevarao, S. Denev, M. D. Biegalski, Y. L. Li, L. Q. Chen, S. Trolier-McKinstry, D. G. Schlom, and V. Gopalan, *Appl. Phys. Lett.* **92**, 192902 (2008).
- ¹⁴R. Wördenweber, E. Hollmann, R. Kutzner, and J. Schubert, *J. Appl. Phys.* **102**, 044119 (2007).
- ¹⁵J. H. Haeni, P. Irvin, W. Chang, R. Uecker, P. Reiche, Y. L. Li, S. Choudhury, W. Tian, M. E. Hawley, B. Craigo, A. K. Tagantsev, X. Q. Pan, S. K. Streiffer, L. Q. Chen, S. W. Kirchoefer, J. Levy, and D. G. Schlom, *Nature (London)* **430**, 758 (2004).
- ¹⁶N. A. Pertsev, A. K. Tagantsev, and N. Setter, *Phys. Rev. B* **61**, R825 (2000); **65**, 219901(E) (2002).
- ¹⁷Y. L. Li, S. Choudhury, J. H. Haeni, M. D. Biegalski, A. Vasudevarao, A. Sharan, H. Z. Ma, J. Levy, V. Gopalan, S. Trolier-McKinstry, D. G. Schlom, Q. X. Jia, and L. Q. Chen, *Phys. Rev. B* **73**, 184112 (2006).
- ¹⁸A. Antons, J. B. Neaton, K. M. Rabe, and D. Vanderbilt, *Phys. Rev. B* **71**, 024102 (2005).
- ¹⁹G. Sheng, Y. L. Li, J. X. Zhang, V. Gopalan, D. G. Schlom, Q. X. Jia, Z. K. Liu, and L. Q. Chen, *Appl. Phys. Lett.* **96**, 232902 (2010).
- ²⁰Y. L. Li, S. Y. Hu, Z. K. Liu, and L. Q. Chen, *Acta Mater.* **50**, 395 (2002).
- ²¹Y. H. Zhang, J. Y. Li, and D. N. Fang, *J. Appl. Phys.* **107**, 034107 (2010).
- ²²A. Kotsos and C. M. Landis, *ASME J. Appl. Mech.* **77**, 041014 (2010).
- ²³A. Artemev, B. Geddes, J. Slutsker, and A. Roytburd, *J. Appl. Phys.* **103**, 074104 (2008).
- ²⁴Y. C. Song, A. K. Soh, and Y. Ni, *J. Phys. D: Appl. Phys.* **40**, 1175 (2007).
- ²⁵C.-H. Lin, C.-M. Huang, and G. Y. Guo, *J. Appl. Phys.* **100**, 084104 (2006).
- ²⁶Y. L. Li, L. Q. Chen, G. Asayama, D. G. Schlom, M. A. Zurbuchen, and S. K. Streiffer, *J. Appl. Phys.* **95**, 6332 (2004).
- ²⁷A. K. Tagantsev, *Ferroelectrics* **375**, 19 (2008).
- ²⁸C. H. Woo and Y. Zheng, *Appl. Phys. A: Mater. Sci. Process.* **91**, 59 (2008).
- ²⁹L. Q. Chen, *Physics of Ferroelectrics* (Springer, Berlin, 2007), Vol. 105, p. 367.
- ³⁰Materials constants for SrTiO₃: $\alpha_1=4.5 \times 10^{-3}[\coth(54/T)-\coth(54/30)]$, $\alpha_{11}=2.1 \times 10^{-12}$, $\alpha_{12}=4.85 \times 10^{-12}$, $\beta_{11}=1.69 \times 10^{43}$, $\beta_{12}=3.88 \times 10^{43}$, $Q_{11}=5.09 \times 10^{-13}$, $Q_{12}=-1.50 \times 10^{-13}$, $Q_{44}=1.065 \times 10^{-13}$, $\Lambda_{11}=8.7 \times 10^{14}$, $\Lambda_{12}=-7.8 \times 10^{14}$, $\Lambda_{44}=-9.2 \times 10^{14}$, $c_{11}=3.36 \times 10^{12}$, $c_{12}=1.07 \times 10^{12}$, $c_{44}=1.27 \times 10^{12}$, $t_{11}=-1.94 \times 10^{15}$, $t_{12}=-0.84 \times 10^{15}$, $t_{44}=6.51 \times 10^{15}$ (in cgs units and T in Kelvin).
- ³¹A. Yamanaka, M. Kataoka, Y. Inaba, K. Inoue, B. Hehlen, and E. Courtens, *Europhys. Lett.* **50**, 688 (2000).
- ³²R. C. Neville, B. Hoeneisen, and C. A. Mead, *J. Appl. Phys.* **43**, 2124 (1972).